

Silver–Zeolite-Modified Electrodes: An Intrazeolite Electron Transport Mechanism

Jian-wei Li, Klaus Pfanner, and Gion Calzaferri*

Institute for Inorganic and Physical Chemistry, University of Berne, Freiestrasse 3,
CH-3000 Berne 9, Switzerland

Received: September 2, 1994; In Final Form: November 1, 1994[⊗]

Ag⁺–A zeolite monograin layers deposited on glassy carbon electrodes show a remarkable electrochemical behavior. The number and the position of peaks and shoulders which appear in cyclic voltammograms during the first cathodic scan depend on the Ag⁺-exchange degree, the scan rate, and the electrolyte cations. Our observations indicate the presence of eight electrochemically distinct silver species. We discuss the mechanism of the electrochemical reactions by assuming site-specific reduction potentials, site-to-site interconversion of Ag⁺ ions, and formation of silver clusters, and we propose an intrazeolite electron transport mechanism. Seven peaks observed in the cyclic voltammograms are related to reduction within the zeolite in an intrazeolite process. One corresponds to an extrazeolite process, namely, the reduction of Ag⁺ ions on the surface of the glassy carbon electrode after ion exchange of Ag⁺ out of the zeolite. Four peaks out of the seven are tentatively assigned to the reduction of Ag⁺ at different sites in the zeolite framework and three to the reduction of silver clusters formed in the α -cage during the cathodic scan.

I. Introduction

Zeolites are appealing host materials owing to the ability of their open crystallites to selectively exchange and incorporate both charged and neutral species within the void spaces and interconnecting channels. Modification of electrodes with zeolite has evoked considerable interest in the past decade.¹ A number of electroactive probes have been investigated at zeolite-modified electrodes, including transition metal ions, complexes, and organic molecules.^{1–7} Two kinds of zeolite coatings on substrate electrodes have been commonly used: porous zeolite/polystyrene layers and carbon powder/zeolite pellets. We have developed a simple method to prepare dense zeolite monograin layers on substrate electrodes,^{2,5,7} and we recently found that electrochemical information useful for mechanistic studies is only obtained from those zeolite particles which directly contact the surface of the substrate electrode.⁷ Shaw and co-workers proposed an intrazeolite and an extrazeolite mechanism to explain the electrochemical processes at zeolite-modified electrodes.⁸ They concluded that intercalated transition metal ions are electrochemically “silent”. This means that the electrochemical reactions occur outside of the zeolite after ion exchange of electroactive species. We, however, found that Ag⁺ ions in zeolite A and Cu²⁺ ions in zeolite Y are electrochemically “active”, and we have proposed an intrazeolite ion transport mechanism for the electrode processes at Cu²⁺–Y-modified electrodes to explain our observations.^{2,7}

Ramos *et al.* were the first to report an electrochemical study at Ag⁺–zeolite-modified electrodes.⁹ They prepared electrodes by compressing a mixture containing Ag⁺–mordenite and graphite on a stainless steel grid and investigated them by chronopotentiometry in aqueous solutions containing various supporting electrolytes. They found that the electrochemical reduction of Ag⁺ ions occurs at the current collector in these experiments which corresponds to an extrazeolite process. Baker and Zhang examined the electrochemical response of Ag⁺–Y-modified electrodes prepared as zeolite/graphite powder/polystyrene layer on ITO glass.⁶ Cathodic linear scan voltammetry at electrodes with low Ag⁺ exchange degree (<10%)

indicated the presence of two electrochemically distinct silver cations. The authors suggested that the two cathodic waves observed are related to occupancy of Ag⁺ ions at sites I and I' in zeolite Y. They reported that the electrochemical processes occur at the surface of the zeolite and that the mechanism of electron transfer to intrazeolite silver cations proceeds via ion exchange of Ag⁺ with electrolyte cations. We found that the cyclic voltammograms of Ag⁺–A zeolite monograin layers on glassy carbon electrodes show a dramatic dependence on the degree of Ag⁺ exchange and that the silver ions in the zeolite are electrochemically active.² We now report detailed cyclic voltammetry studies at these systems, and we propose an intrazeolite electron transport mechanism.

II. Experimental Section

Materials and Chemicals. Zeolite A (Linde 4A, Baylith T, Bayer) was equilibrated for 3 days at ambient air before use, and its composition was analyzed by Ciba-Geigy AG. The unit cell composition is Na₁₂(AlO₂)₁₂(SiO₂)₁₂·7.6H₂O. All chemicals were analytical grade and were used as received. Double-distilled water was used in all experiments.

Instrumentation. Electrochemical experiments were carried out in a standard one-compartment, three-electrode cell with a water jacket for connection to a thermostatic water circulator. The counter electrode was a Pt sheet electrode. The reference electrode was a saturated calomel electrode (SCE) with a 1 M NaNO₃ bridge electrolyte solution and a Vycor frit to avoid the influence of Cl[–] ions. The potentials were referred to this electrode (SCE) and not corrected for *iR* drop and liquid junction potentials. The electrolyte solution was purged with Ar for at least 20 min before starting the measurements. The voltammetric measurements were carried out immediately after immersion of the electrode into the electrolyte solution at 20 °C. The surface of the electrolyte solution was protected by Ar during the measurements. Voltammetric experiments were performed with EG&G Model 273 potentiostat and Model 270 electrochemical analysis system.

Potentiometry measurements were carried out with an Ag⁺ ion-selective electrode (Model IS 550-Ag⁺, Philips) and a saturated calomel electrode with a bridge electrolyte solution

* To whom correspondence should be addressed.

[⊗] Abstract published in *Advance ACS Abstracts*, January 15, 1995.

(RE 3/DJ, Philips). The bridge electrolyte solution was 1 M NaNO₃ to avoid the influence of Cl⁻. The emf measurements were performed with a potentiometer (PW 9422 pH meter, Philips).

Atomic absorption analysis of silver was performed with an atomic absorption spectrophotometer (Beckman, 1248).

Calibration of the Ag⁺ Ion-Selective Electrode. The concentration of Ag⁺ in solution was determined with an Ag⁺ ion selective electrode in the dark. Approximately 200 mL of 1.000 M NaNO₃ was added to a cell (about 400 mL) with a water jacket for connection to a thermostatic water circulator and stirred magnetically for about half an hour in order to reach a constant temperature of 20 °C. A 20 μL aliquot of 1.000 M AgNO₃ was added to the above solution with a micropipet, and the emf was measured under continuous stirring. This operation was repeated until the concentration of Ag⁺ was 1.00 mM.

Kinetics of the Ag⁺ Exchange into Zeolite A. A 9.10 mg sample of zeolite A was added to the above solution containing 1.000 M NaNO₃ and 1.00 mM AgNO₃. The emf's were measured with the calibrated Ag⁺ ion-selective electrode under continuous stirring at different times, *t* = 1, 2, 4, 6, 8, 10, 20, 40, and 60 min.

Electrode Preparation and Ion Exchange. Glassy carbon disk electrodes of 3.0 mm diameter were used as substrate electrodes. The zeolite-modified electrodes were prepared as described elsewhere.⁷ The coatings contained 20 μg of zeolite and *ca.* 0.2 μg of polystyrene.

The Ag⁺-A-modified glassy carbon electrodes with different Ag⁺-exchange degree were prepared by the following procedure: Prior to Ag⁺ ion exchange, the Na-A-modified electrodes were cleaned by rotating at 500 rpm in 0.1 M NaNO₃ solution for 10 min and washed with double-distilled water. The so-prepared electrodes were ion-exchanged in 200 mL of NaNO₃ + AgNO₃ solution under rotation at 500 rpm at 20 ± 1 °C in the dark for 30 min and washed thoroughly with double-distilled water to obtain partially Ag⁺-exchanged Ag⁺-A-modified electrodes. The initial concentrations of AgNO₃, [Ag⁺]_s⁰, were 0.05, 0.1, and 0.3 mM, and the initial concentration of NaNO₃, [Na⁺]_s⁰, was 0.1 M; that is, the ratios [Ag⁺]_s⁰/[Na⁺]_s⁰ in the solutions were 5 × 10⁻⁴, 1 × 10⁻³, and 3 × 10⁻³, respectively. To obtain fully Ag⁺-exchanged samples, ion exchange was carried out in 0.1 M AgNO₃ under otherwise the same conditions.

Determination of the Ag⁺-Exchange Degree. The Ag⁺-exchange degree of the Ag⁺-A-modified electrodes was determined by atomic absorption spectrophotometry. For each Ag⁺-exchange degree, nine electrodes were prepared, and their zeolite layers were dissolved ultrasonically in 10 mL of 1.0 M HNO₃. The concentration of Ag⁺ was measured using 1.0 M HNO₃ as a reference.

III. Results and Discussion

Kinetics of Ag⁺ Exchange. The calibration curve of the Ag⁺ ion-selective electrode was determined in 200 mL of a 1.000 M NaNO₃ solution at 20 °C from 0.1 to 1.0 mM AgNO₃. It was linear with a slope of 58.14 mV and a correlation coefficient of 0.99998. The concentration of Ag⁺ in the aqueous phase, [Ag⁺]_s, decreases with time after addition of 9.10 mg of zeolite A to a solution containing 1.000 M NaNO₃ and 1.00 mM AgNO₃ because the Ag⁺ ions are exchanged into the zeolite. The Ag⁺-exchange degree *X* in percent can be calculated as

$$X = \frac{([Ag^+]_s^0 - [Ag^+]_s)V_s M_z(100)}{W_z Z} \% \quad (1)$$

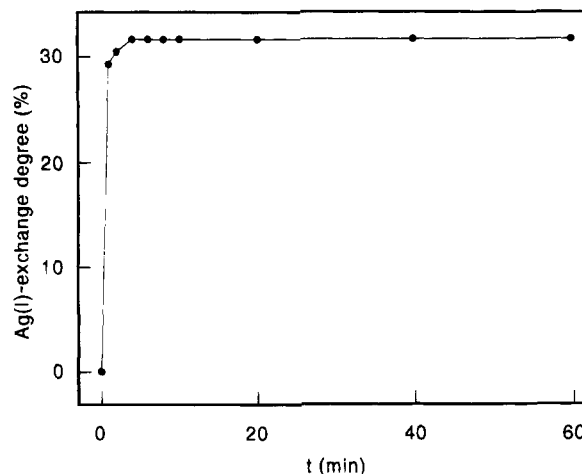


Figure 1. Ag⁺-exchange degree of zeolite A as a function of the exchange time at 20 °C. A 9.1 mg sample of zeolite A was added to 200 mL of an aqueous 1.000 M NaNO₃ + 1.00 M AgNO₃ solution.

[Ag⁺]_s⁰ and [Ag⁺]_s are the initial molar concentration in the aqueous phase and the concentration at exchange time *t*, respectively. *V*_s, *W*_z, *M*_z, and *Z* are the volume of the aqueous phase in dm³, the weight of added zeolite in grams, the formula weight of the unit cell of zeolite in g mol⁻¹, and the negative charge of the zeolite unit cell, respectively. In Figure 1 we show *X* as a function of time. The results indicate that the Ag⁺/Na⁺ ion-exchange equilibrium is reached in about 10 min under the experimental conditions. An ion-exchange time of 30 min was chosen to prepare the monograin Ag⁺-A-modified glassy carbon electrodes based on this finding.

Ion-Exchange Equilibrium and Ag⁺-Exchange Degree. In Figure 1 *X* reaches a maximum value of 32% at ion-exchange equilibrium. This corresponds to an apparent selectivity coefficient *K*_{Na⁺Ag⁺}^{Ag} of 514.

$$K_{Na}^{Ag} = \frac{[Ag^+]_z^* [Na^+]_s^*}{[Ag^+]_s^* [Na^+]_z^*} \quad (2)$$

The asterisk represents equilibrium concentrations. Since *X* can be expressed as

$$X = \frac{[Ag^+]_z^*}{[Ag^+]_z^* + [Na^+]_z^*} \times 100\% \quad (3)$$

substitution of [Ag⁺]_z^{*}/[Na⁺]_z^{*} in (2) leads to

$$K_{Na}^{Ag} = \frac{[Na^+]_s^* X}{[Ag^+]_s^* (100 - X)} \quad (4)$$

The amount of Ag⁺ exchanged to the zeolite A layer is considerably smaller than the total amount of Ag⁺ in the solution under the applied conditions. The concentration changes of Ag⁺ and Na⁺ in the solutions are therefore negligible. This means that [Ag⁺]_s^{*} = [Ag⁺]_s⁰ and [Na⁺]_s^{*} = [Na⁺]_s⁰ holds and that eq 4 can be written as

$$K_{Na}^{Ag} = \frac{[Na^+]_s^0 X}{[Ag^+]_s^0 (100 - X)} \quad (5)$$

X can therefore be estimated from eq 5, the measured apparent selectivity coefficient, and the [Ag⁺]_s⁰/[Na⁺]_s⁰ ratio. The values in Table 1 show close agreement with the atomic absorption spectrophotometry (AAS) data for small [Ag⁺]/[Na⁺] ratios. A

TABLE 1: Ag⁺-Exchange Degree of Ag⁺-A-Modified Glassy Carbon Electrodes

electrode	$[\text{Ag}^+]_s^0/[\text{Na}^+]_s^{0a}$	X_c (%) ^b	X_m (%) ^c	x^d
1	5×10^{-4}	20	22	2.6
2	1×10^{-3}	34	33	4.0
3	3×10^{-3}	61	54	6.5
4		100	100	12

^a Ratios in the solutions to prepare the Ag⁺-A-modified electrodes. The Na⁺ concentration was always 0.100 M. ^b X_c is the Ag⁺-exchange degree in percent derived from eq 5. ^c X_m is the Ag⁺-exchange degree in percent measured by atomic absorption spectrophotometry. ^d x is the stoichiometric exchange degree for Ag_{*x*}Na_{12-*x*}-A and is based on X_m .

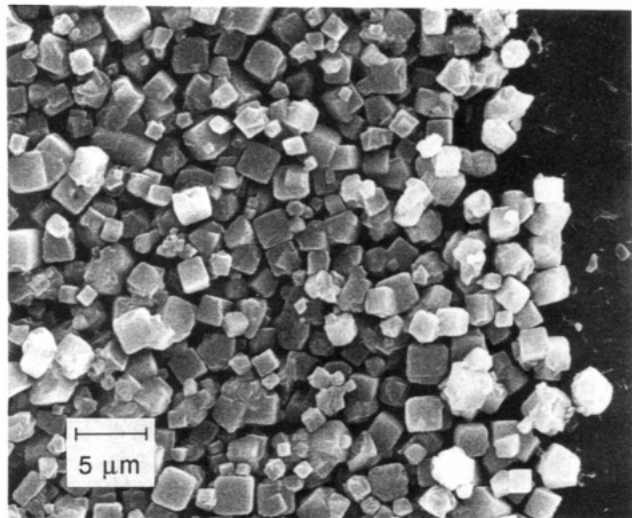


Figure 2. SEM micrograph of a Na₁₂-A zeolite layer on a glassy carbon disk electrode. The uncoated part on the right side represents the surface of the glassy carbon electrode.

deviation of 13% is observed for electrode 3. The concentration of Na⁺ ions is 0.100 M, and that of Ag⁺ is much smaller in each case. We can therefore assume that the activity coefficients of Na⁺ and of Ag⁺ are the same in all solutions and remain constant during the ion exchange. This means that the deviations of X as derived from (5) with respect to the values obtained by AAS are mainly due to the activity coefficients of Ag⁺ and Na⁺ in the zeolite.

The Ag⁺-exchanged zeolite A is represented as Ag_{*x*}Na_{12-*x*}-A where the stoichiometric exchange degree x can be calculated from X . The x values 2.6, 4.0, 6.5, and 12 reported in Table 1, as determined by AAS, are used in the following text.

Zeolite Layer Structure. The texture of a typical Na-A zeolite layer on a glassy carbon electrode obtained by scanning electron microscopy (SEM) is shown in Figure 2. The uncoated part on the right side represents the surface of the glassy carbon electrode, where the zeolite coating was carefully peeled off before performing SEM in order to give a clear view of the thickness of the zeolite layer. It shows that the coating achieved by our procedure consists of one to two condensed monograin layers of about 1 μm³ zeolite particles and that the thickness of the zeolite layer is in the order of 1 μm. The zeolite layers are mechanically stable. No apparent loss of zeolite from the surface of the glassy carbon electrode in aqueous solution has been observed even under rotation at 3000 rpm. The experimental reproducibility obtained with this kind of zeolite-modified electrodes is good.⁷

Voltammetric Behavior of Ag⁺-A-Modified Electrodes. Cyclic voltammograms of monograin Ag⁺-A-modified electrodes have been measured in 0.1 M LiClO₄ and in 0.1 M NaClO₄ at different scan rates and different Ag⁺-exchange degrees x in a systematic way. Electrodes prepared in exactly the same way have been investigated in the two electrolytes,

so that the results illustrated in Figures 3 and 4 can be compared with each other. In these two figures each column corresponds to a different x but the same scan rate, and each row corresponds to a different scan rate but the same x . A dramatic dependence of the peaks and shoulders on x , the scan rate, and the electrolyte cation is apparent. The peaks and shoulders indicate the presence of eight electrochemically distinct silver species which we denote as A through H.

We distinguish three possible reaction sites, i.e., the uncovered part of the substrate electrode surface, the substrate electrode/solution/zeolite interface, and the cages and channels of the zeolite. The influence of the ion-exchange capability of zeolites on electrode processes was discussed by us in a study at monograin Cu²⁺-Y-modified electrodes. We found for this system that the electrochemical processes occur at the zeolite side of the glassy carbon/solution/zeolite interface, which corresponds to an intrazeolite ion transport mechanism.⁷

Structured voltammograms of silver at gold and platinum electrodes were reported by Sandoz et al. and attributed to surface effects.¹⁰ The question arises if our structured voltammograms can be explained by a similar effect because Ag⁺ ion exchange with the electrolyte cations occurs after inserting an Ag⁺-A-modified electrode into an electrolyte solution. We have therefore carried out voltammetric experiments at naked glassy carbon electrodes in the Ag⁺ concentration range from 0.87 to 15.5 mM in 0.1 M LiClO₄ at 10 mV/s. Only one cathodic peak at 0.15 V vs SCE with currents in the range from 7.71 to 128 μA was observed. These currents are comparable to those observed at Ag⁺-A-modified electrodes at a scan rate of 10 mV/s as reported in Figure 3. As an example, we compare the cathodic peak measured at the blank glassy carbon electrode in 1.0 mM AgNO₃ + 0.1 M LiClO₄ with the first cathodic wave of the Ag₁₂-A-modified electrode in 0.1 M LiClO₄; see Figure 5. The cathodic peak at the blank glassy carbon electrode matches H exactly. This proves that the peaks A to G are not due to reduction of leached Ag⁺ at the uncovered part of the surface of the glassy carbon electrode.

Can the peaks A to G be explained by assuming Ag⁺ reduction at the zeolite side of the glassy carbon/solution/zeolite interface as observed for the Cu²⁺-Y-modified electrodes? Ion exchange occurs, and x decreases as soon as an Ag⁺-A-modified electrode is inserted into the electrolyte. Decreasing scan rate means also increasing immersion time, and hence the amount of Ag⁺ ions leached out of the zeolite during the first cathodic scan increases. Thus, the Ag⁺ concentration in the zeolite is larger at high scan rates than at low ones at a constant initial x . Increasing initial x at constant scan rate should cause a similar pattern as an increasing scan rate at constant initial x if A to G would result from an electrode process at the zeolite side of the glassy carbon/solution/zeolite interface. This is not, however, what we observed. The electrodes respond at more positive potential at large x and low scan rate and at more negative potential at small x and high scan rate in a systematic way, as shown in Figures 3 and 4. In the following we explain that it is reasonable to assume an intrazeolite electron transport process in which reduction of Ag⁺ ions takes place within the cages and channels of the zeolite.

Site-Specific Reduction Potentials. Scheme 1 shows crystallographically identified cation positions of zeolite A. Site SII is at the center of a 6-ring face with sites SII' and SII* displaced into and out of the β-cage along the triad axis, respectively, while site SIII is adjacent to the 4-ring in the α-cage. Site SV, which is not indicated in Scheme 1, is at the center of the octagonal window. In fully hydrated Ag₁₂-A, Ag⁺ ions are located at these four different sites.^{11,12} Kim and Seff indicated that in fully hydrated A zeolite the coordination

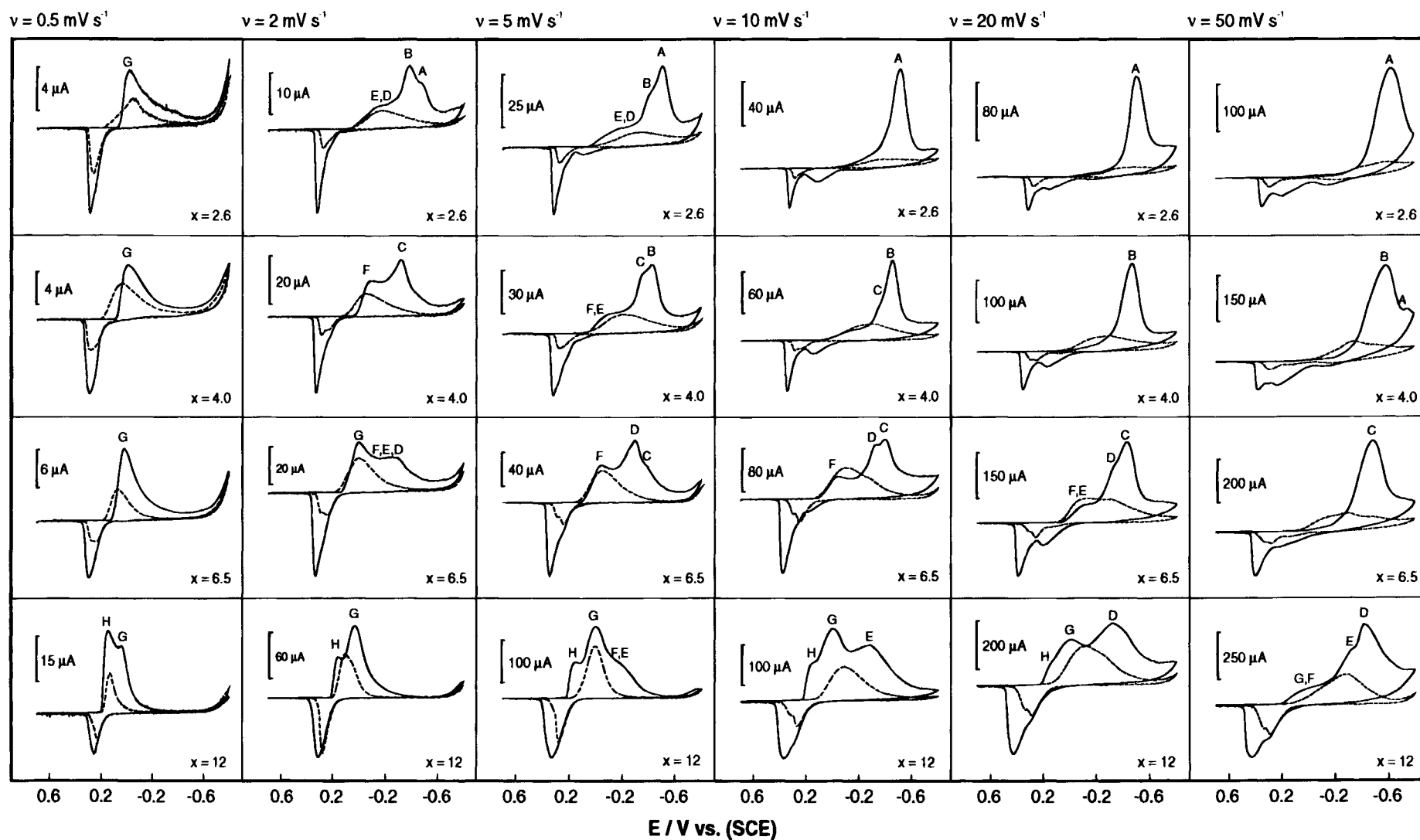


Figure 3. Voltammetric behavior of Ag^+ -A-modified glassy carbon electrodes in 0.1 M LiClO_4 at 20 °C as a function of the scan rate and the Ag^+ -exchange degree x . Each column corresponds to a different x but the same scan rate, and each row corresponds to a different scan rate but the same x . The solid and dashed lines are the first and the second cycles, respectively. The upper half of traces are the cathodic currents. The initial potential is 0.7 V and the switching potential is -0.8 V.

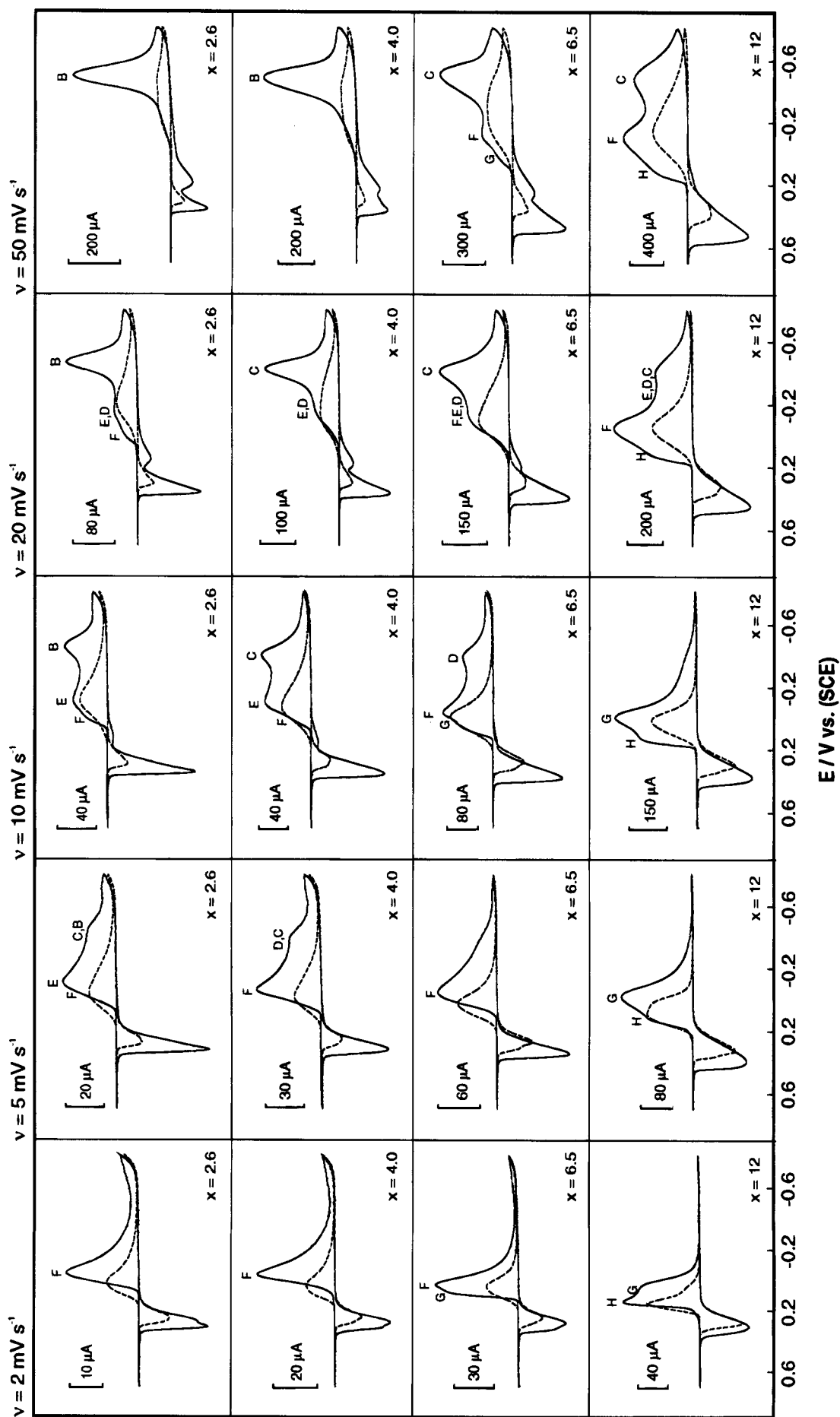
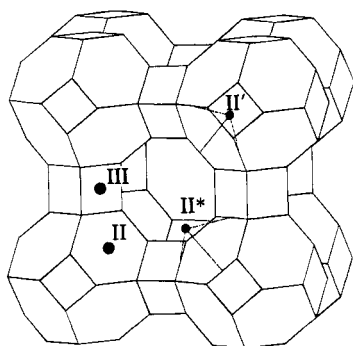


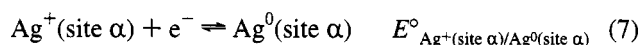
Figure 4. Voltammetric behavior of Ag^+ -A-modified glassy carbon electrodes in 0.1 M NaClO_4 as a function of the scan rate and the Ag^+ -exchange degree. The conditions are otherwise the same as in Figure 3.

SCHEME 1: Structure of Zeolite A Showing Crystallographically Identified Cation Positions

strength of Ag^+ at different sites decreases in the order¹¹

$$\text{Ag}^+(\text{SII}') > \text{Ag}^+(\text{SII}^*) \gg \text{Ag}^+(\text{SV}) \sim \text{Ag}^+(\text{SIII}) \quad (6)$$

They also reported that Ag^+ at the sites SIII and SV are very weakly coordinated to the zeolite framework and that the Ag^+ at SIII are easier to be reduced than those at SV. It is reasonable to assume that Ag^+ ions at different sites possess different redox potentials and that less adequately coordinated ions are easier to be reduced. In addition, the size of clusters that can form at different sites is different. It is therefore appealing to express the reduction potential for a site α as



We assume that the site-specific reduction potentials $E^\circ_{\text{Ag}^+(\text{site } \alpha)/\text{Ag}^0(\text{site } \alpha)}$ decrease in the order

$$E^\circ(\text{SII}') < E^\circ(\text{SII}^*) \ll E^\circ(\text{SV}) < E^\circ(\text{SIII}) \quad (8)$$

Site-to-Site Interconversion of Ag^+ . We consider the following Ag^+ distribution equilibrium at the different sites of the zeolite:



The number of Ag^+ at each site depends on the number of positions available, on site preference, and on the Ag^+ -exchange degree. In fully hydrated $\text{Ag}_{12}\text{-A}$, three Ag^+ are located on 3-fold axes (SII') where they are bridged by three water molecules within the sodalite unit, five occupy 3-fold-axis positions near 6-rings, recessed by 0.86 Å into the large cavity from 111 planes (SII*), three are associated with the eight oxygen rings (SV), and the remaining one is located at SIII.¹¹ On the basis of experimental and theoretical evidence,^{13,14} we assume that the Ag^+ ions are mainly located at SII' when $x \leq 3$ and that SII* and SV are filled up next until $x = 8$ and $x = 11$, respectively, is reached. When equilibrium (9) is disturbed, a site-to-site interconversion of Ag^+ happens until a new equilibrium is established.

Peak H. We have already discussed that peak H in Figures 3–5 results from reduction of leached Ag^+ ions at the uncovered part of the surface of the glassy carbon electrode. This is further supported by the following reasoning. After inserting an $\text{Ag}^+\text{-A}$ -modified electrode into a solution, Ag^+ ions are ion-exchanged out of the zeolite into solution by electrolyte cations. The rate of Ag^+ leaching out of the zeolite depends on the initial degree of Ag^+ exchange, the cocations, and the electrolyte cations. Ag^+ ions at different sites in zeolites have been reported to possess different mobilities during ion exchange in the sense that bound ions are first converted to mobile ions in the large cavities and then diffuse rapidly through the main channels to the zeolite surface.^{15–17} We assume that the stronger the ions are coordinated to the zeolite framework, the more time it takes to convert them to mobile ions. The diffusion rate

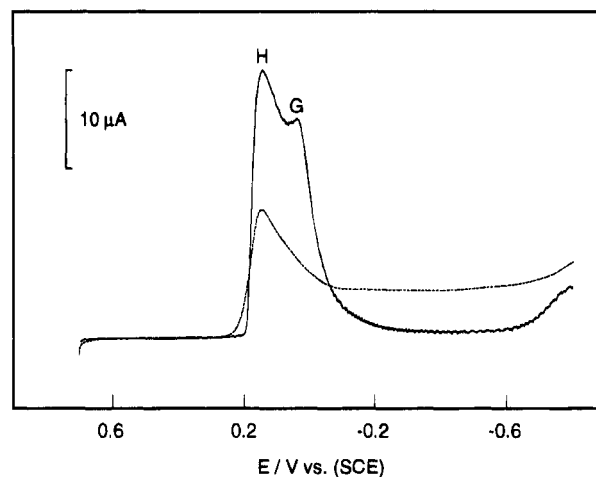


Figure 5. Comparison of the cathodic behavior of the $\text{Ag}_{12}\text{-A}$ -modified glassy carbon electrode and that of Ag^+ ions at the blank glassy carbon electrode: solid line, $\text{Ag}_{12}\text{-A}$ -modified glassy carbon electrode in 0.1 M LiClO_4 at 20 °C at a scan rate of 0.5 mV s^{-1} ; dashed line, blank glassy carbon electrode in 0.1 M LiClO_4 + 1.0 mM AgNO_3 at 20 °C at a scan rate of 10 mV s^{-1} .

depends also on the concentration gradient. The larger x is, the larger the concentration gradient at the zeolite/solution interface. Since the Ag^+ ions prefer the sites SII' and SII* at which they are most strongly coordinated, they are mainly located at these two sites when $x \leq 8$. With increasing exchange degree ($x > 8$), more and more Ag^+ occupy sites SV and SIII at which they become mobile easily. At lower scan rate, there is more time for this leaching process. This explains why H is only observed at $\text{Ag}_{12}\text{-A}$ -modified electrodes in both electrolytes and why its relative height decreases with respect to G with increasing scan rate.

Peaks A to G. The peaks G, F, E, ..., A show up in this order at more and more negative potential, and their appearance strongly depends on the Ag^+ -exchange degree x , the scan rate, and the electrolyte cation. The frequency and the intensity of the more negative potential peaks increase with decreasing x and increasing scan rate in a systematic way. The most negative one, A, is only observed in the LiClO_4 electrolyte and at small x , B is the most negative potential peak in NaClO_4 , while all other peaks appear in both electrolytes. The site-specific reduction potentials (7), the site-to-site interconversion reactions (9), and the formation of silver clusters can account for these observations.

When an $\text{Ag}^+\text{-A}$ -modified electrode is inserted into the electrolyte solution and/or Ag^+ ions start to be reduced, equilibrium (9) is disturbed, and site-to-site interconversion starts to play an increasingly important role. This process is less material at small x and high scan rate. Mainly Ag^+ ions located at their original equilibrium sites are reduced at fast scan rates, with respect to the time scale of the Ag^+ interconversion (9). This explains why the negative potential cathodic peaks dominate at low x .

The electrolyte cations move into the zeolite during the cathodic process to maintain charge neutrality. They then act as co-cations and migrate to the corresponding sites in the Ag^+ site-to-site interconversion process, which depends on their mobility; e.g., the migration of Li^+ ions through the 6-rings is more difficult than that of Na^+ .¹⁵ We have recently shown that the electrode processes at $\text{Cu}^{2+}\text{-Y}$ -modified electrodes are much influenced by electrolyte alkali cations and that in this system the mobility of Li^+ is much lower than that of Na^+ , K^+ , and Cs^+ .⁷ The general positive shift of the cathodic waves in the Na^+ electrolyte with respect to the Li^+ electrolyte and the disappearance of peak A in the former case are therefore plausible.

The most negative peak A is only observed in Figure 3 and at low x . It becomes dominant at $x = 2.6$ when $\nu \geq 5$ mV/s. This means that the scan rate is fast enough with respect to the time scale of the interconversion of Ag^+ under these conditions and that the Ag^+ ions are mainly reduced at their original sites SII' which are located in the β -cage. In the NaClO_4 electrolyte, however, it seems that even the scan rate 50 mV/s is not fast enough to compete with the Ag^+ interconversion rate because of the larger mobility of Na^+ with respect to Li^+ . This explains why peak A is missing in this electrolyte.

B appears at low x in both electrolytes. In LiClO_4 at $x = 4.0$ and $\nu = 20$ mV s^{-1} only peak B is observed, while it appears together with a small peak A at $x = 4.0$ and $\nu = 50$ mV s^{-1} . We assume that the interconversion of $\text{Ag}^+(\text{SII}') to $\text{Ag}^+(\text{SII}^*)$ is faster than that of $\text{Ag}^+(\text{SII}') and $\text{Ag}^+(\text{SII}^*) to $\text{Ag}^+(\text{SV})$ and $\text{Ag}^+(\text{SIII})$, because the sites SII' and SII* are close to each other and the Ag^+ coordination strength is larger than at SV and SIII. If the scan rate is fast enough with respect to the time scale of the $\text{Ag}^+(\text{SII}') and $\text{Ag}^+(\text{SII}^*) to $\text{Ag}^+(\text{SV})$ and $\text{Ag}^+(\text{SIII})$ interconversion and slow enough with respect to the time scale of the $\text{Ag}^+(\text{SII}') to $\text{Ag}^+(\text{SII}^*)$ interconversion, then reduction of Ag^+ will only happen at SII*. In this case only one less negative peak compared to A should be observed. If not all Ag^+ ions at SII' can switch to SII* above a critical scan rate, both peaks B and A are expected. This reasoning is in agreement with the observations, and we therefore assign B to the reduction of Ag^+ ions at SII*.$$$$$$

G dominates at $x < 8$ and $\nu = 0.5$ mV s^{-1} in Figure 3. According to (8), the Ag^+ ions at SIII are reduced first. If the scan rate is slow enough relative to the time scale of both, the site-to-site interconversion, and the migration of silver clusters, only the Ag^+ ions at this site are reduced, and hence only one most positive peak can be observed. On the basis of this we assign peak G to the reduction of Ag^+ ions at SIII.

F appears as the first peak and with a large current at $x = 4.0$ and $\nu = 2$ mV s^{-1} , at $x = 6.5$ and $\nu = 5$ and 10 mV s^{-1} in Figure 3, and at $x \leq 6.5$ and $\nu \leq 5$ mV s^{-1} in Figure 4. Such a large current can only result from the reduction of a large amount of Ag^+ ions or charged silver clusters. However, the formation of such a large amount of charged silver clusters needs many Ag^0 atoms which must be produced before peak F can develop. This indicates that F does not correspond to the reduction of charged silver clusters, and it seems reasonable to assign F to the reduction of Ag^+ ions at SV according to (8).

We have assigned A, B, F, G, and H to the reduction of Ag^+ ions at the sites SII', SII*, SV, and SIII and at the glassy carbon electrode, respectively. What remains are C, D, and E. We can speculate that during the first cathodic scan the produced Ag^0 atoms react with each other and with unreduced Ag^+ to form uncharged and charged silver clusters, Ag_n^{m+} ($m < n$), with different redox ability. Uncharged silver clusters may migrate out of the zeolite.^{5,17,18} The formation of silver clusters Ag_n^{m+} in zeolite A has been investigated considerably.^{19,20} The maximum value of n is limited by the size of the zeolite cages. In addition, it was experimentally and theoretically found that the redox ability of silver clusters depends on their size.²¹⁻²⁴ On the basis of this it makes sense to allege C, D, and E to the reduction of silver clusters formed during the cathodic scan. However, we have no detailed information about these cluster so far.

Charges in the First Cathodic Processes. Voltammetry experiments of Na_{12} -A-modified electrodes have been carried out under the same conditions as those reported in Figures 3 and 4. No peaks have been observed at any scan rate in both electrolytes. The nonfaradaic charges in the cathodic process have been obtained by integrating the cathodic curves. The total

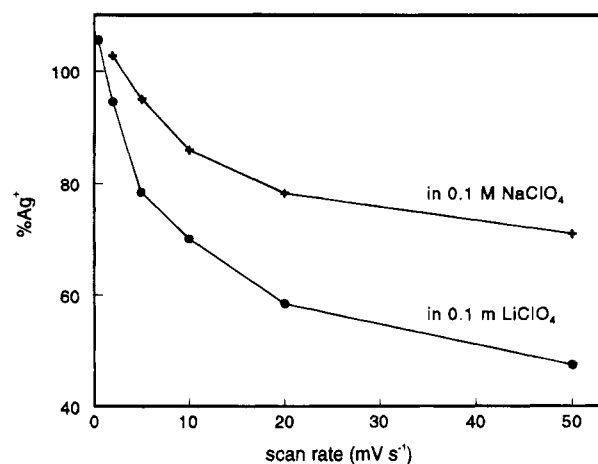


Figure 6. Percentage of reduced Ag^+ ions ($\% \text{Ag}^+$) on the Ag_4Na_8 -A zeolite-modified electrodes during the first cathodic scan as a function of the scan rate.

charges (faradaic + nonfaradaic) produced in the first cathodic scan were obtained in the same way for Ag^+ -A-modified electrodes. The faradaic charges of the first cathodic scans can be obtained by assuming that the charging current is the same for both types of electrodes. The percentage of the silver ions ($\% \text{Ag}^+$) reduced during the first cathodic scan can then be calculated from the measured faradaic charge, the amount of the zeolite on the electrode (20 μg), and the Ag^+ -exchange degree.

The $\% \text{Ag}^+$ reduced as a function of the scan rate is shown in Figure 6 for the Ag_4Na_8 -A-modified electrode in 0.1 M LiClO_4 and in 0.1 M NaClO_4 . More than 100% have been observed at $\nu = 0.5$ mV s^{-1} in 0.1 M LiClO_4 and at $\nu = 2$ mV s^{-1} in 0.1 M NaClO_4 . This may be caused by the different charging currents of the Ag_4Na_8 -A and the Na_{12} -A electrodes. The strong dependence of $\% \text{Ag}^+$ reduced on the scan rate and on the electrolyte cation further indicates that the electrolyte cations play an important role in the cathodic process which is kinetically influenced by the transport of electrolyte cations into the zeolite and their migration in the channels and cavities of the zeolite.

Electrode Response during the Second Cathodic Scan.

The electrode response during the second cathodic scan is completely different from that during the first cathodic scan as shown in Figures 3 and 4. Only one cathodic wave is observed which is broader at small Ag^+ -exchange degree x and high scan rate than at large x and slow scan rate. The electrodes respond in the more negative potential range with decreasing x and increasing scan rate. The current decreases dramatically in the second cycles. It decreases faster at small than at large x , and it decreases faster at high than at slow scan rates.

The second cathodic wave appears mainly in the potential region of the C, D, and E peaks, and they appear at more positive potential with increasing x . This indicates that electrochemical reduction of silver clusters formed during the first cathodic scan occurs and that at larger x larger clusters are formed.

What is the reason for the dramatic decrease of the current in the second cycles which is faster at small than at large x ? Nearly the same percentage of Ag^+ ions are reduced during the first cathodic scan for all Ag^+ -exchange degrees at a given scan rate. This can be explained if we assume that the decrease of the current in the second cycle is mainly caused by migration of uncharged silver clusters out of the zeolite to form electrochemically "silent" silver particles at the zeolite surface.^{5,20} Provided that the smaller uncharged silver clusters migrate faster than the larger ones,¹⁸ the current of the second cycle is expected to decrease faster at low exchange degree and high scan rate.

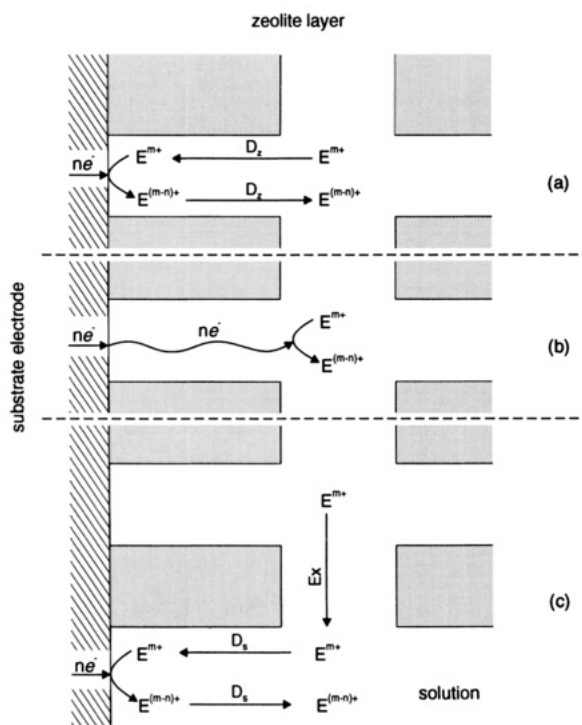


Figure 7. Three possible mechanisms at zeolite-modified electrodes: (a) intrazeolite ion transport mechanism, (b) intrazeolite electron transport mechanism, and (c) extrazeolite mechanism. D_z and D_s represent the diffusion of ions within the zeolite and in solution, respectively. Ex indicates ion exchange at the zeolite/solution interface. The diffusion of cocations within the zeolite and ion exchange of electrolyte cations at the zeolite/solution interface are not indicated.

IV. Conclusions

The voltammetric compartment of Ag^+ -A-modified electrodes depends considerably on the Ag^+ -exchange degree, the scan rate, and the electrolyte cations. Eight electrochemically distinct waves in the first cathodic scans denoted as A through H have been observed. Reduction of Ag^+ ions at different sites of the zeolite and reduction of silver clusters in the zeolite are responsible for the appearance of A to G. These waves are due to intrazeolite processes in which electron transfer takes place within the zeolite. The electrochemistry of the Ag^+ -A-modified electrodes is distinctly different from that observed at Cu^{2+} -Y-modified electrodes at which an intrazeolite ion transport mechanism was proposed.⁷ In this process the electroactive species E^{m+} are reduced after diffusion from the bulk zeolite to the interface substrate electrode/solution/zeolite, and then the reduced species $\text{E}^{(m-n)+}$ diffuse from the interface to the bulk zeolite, as shown in Figure 7a. The electrode processes at Ag^+ -A-modified electrodes, however, are better described as intrazeolite electron transport mechanism as illustrated in Figure 7b. In this mechanism, the electroactive species E^{m+} are reduced at the sites where they are located within the zeolite. This demands sufficient electron conductivity mainly through the channels of the zeolite. Band structure calculations of silver clusters in the cages of zeolites indicate that their interactions are sufficient for such a mechanism to take place.²⁵ Similar results have been obtained for silver halide containing sodalites.²⁶ The mechanism is also supported by our finding that cyclic voltammograms of zeolite A monograin layers on glassy carbon containing occluded silver chloride complexes show quasi-reversible behavior in the dark and under illumination.²⁷ Only peak H corresponds to the extrazeolite process in Figure 7c, namely, the reduction of the leached Ag^+ ions on the substrate electrode. Generally speaking, the E^{m+} ions are ion-exchanged by electrolyte cations into the solution

in an extrazeolite process and then diffuse to the substrate electrode where they are reduced.

Acknowledgment. We thank Professor R. Giovanoli and his staff of the Electron Microscopy Laboratory, University of Bern, for SEM and XRD measurements. This research is part of Project NF 20-34042.92, financed by the Schweizerische Nationalfonds zur Förderung der wissenschaftlichen Forschung, and Project BEW-EPA 217.307, financed by the Schweizerische Bundesamt für Energiewirtschaft.

References and Notes

- Rolison, D. R. *Chem. Rev.* **1990**, *90*, 867 and references therein.
- Li, J.; Calzaferri, G. *J. Chem. Soc., Chem. Commun.* **1993**, 1430.
- Baker, M. D.; Senaratne, C.; Zhang, J. *J. Chem. Soc., Faraday Trans.* **1992**, *88*, 3187.
- Gaillon, L.; Sajot, N.; Bedioui, F.; Devynck, J. *J. Electroanal. Chem.* **1993**, *345*, 157. Xu, M.; Horsthemke, W.; Schell, M. *Electrochim. Acta* **1993**, *38*, 919. Senaratne, C.; Baker, M. D. *J. Electroanal. Chem.* **1992**, *332*, 357. Baker, M. D.; Senaratne, C. *Anal. Chem.* **1992**, *64*, 697. Bharathi, S.; Phani, K. L. N.; Joseph, J.; Pitchumani, S.; Jeyakumar, D.; Rao, G. P.; Rangarajan, S. K. *J. Electroanal. Chem.* **1992**, *334*, 145. Phani, K. L. N.; Pitchumani, S. *Electrochim. Acta* **1992**, *37*, 2411. Cassidy, J.; Breen, W.; O'Donoghue, E.; Lyons, M. E. G. *Electrochim. Acta* **1991**, *36*, 383. Bedioui, F.; De Boysson, E.; Devynck, J.; Balkus, Jr., K. J. *J. Chem. Soc., Faraday Trans.* **1991**, *87*, 3831. Bedioui, F.; De Boysson, E.; Devynck, J.; Balkus, Jr., K. J. *J. Electroanal. Chem.* **1991**, *315*, 313.
- Calzaferri, G.; Hädener, K.; Li, J. *J. Chem. Soc., Chem. Commun.* **1991**, 653.
- Baker, M. D.; Zhang, J. *J. Phys. Chem.* **1990**, *94*, 8703. Baker, M. D.; Senaratne, C.; Zhang, J. *J. Phys. Chem.* **1994**, *98*, 1668.
- Li, J.; Calzaferri, G. *J. Electroanal. Chem.* **1994**, *377*, 163.
- Shaw, B. R.; Creasy, K. E.; Lanczycki, C. J.; Sargeant, J. A.; Tirhado, M. J. *Electrochem. Soc.* **1988**, *135*, 869.
- Pereira-Ramos, J.-P.; Messina, R.; Perichon, J. *J. Electroanal. Chem.* **1983**, *146*, 157.
- Sandoz, D. P.; Peekema, R. M.; Freund, H.; Morrison, C. F., Jr. *J. Electroanal. Chem.* **1970**, *24*, 165.
- Kim, Y.; Seff, K. *J. Phys. Chem.* **1978**, *82*, 1071.
- Thoni, W. Z. *Kristallogr.* **1975**, *142*, 142.
- Schollner, R.; Notzel, P. *Adsorption of Hydrocarbons in Zeolite*, Preprints of the Workshop; Akademie der Wissenschaften DDR: Berlin, 1979; Vol 2.
- Aomura, K. *Sekiyu Gakkaishi* **1987**, *30*, 378.
- Breck, D. W. *Zeolite Molecular Sieves*; John Wiley & Sons: New York, 1974.
- Brown, L. M.; Sherry, H. S.; Krambeck, F. J. *J. Phys. Chem.* **1971**, *75*, 3846.
- Sherry, H. S. *Molecular Sieve Zeolites*; Adv. Chem. Ser. 101; American Chemical Society: Washington, DC, 1971.
- Kim, Y.; Seff, K. *Bull. Korean Chem. Soc.* **1987**, *8*, 69. Sun, T.; Seff, K. *Chem. Rev.* **1994**, *94*, 857.
- Baba, T.; Akinaka, N.; Nomura, M.; Ono, Y. *J. Chem. Soc., Faraday Trans.* **1993**, *89*, 595. Michalik, J.; Wasowicz, T.; van der Pol, A.; Reijerse, E. J.; de Boer, E. *J. Chem. Soc., Chem. Commun.* **1992**, 29. Schoonheydt, R. A.; Leeman, H. *J. Phys. Chem.* **1989**, *93*, 2048. Texter, J.; Kellerman, R.; Gonsiorowski, T. *J. Phys. Chem.* **1986**, *90*, 2118. Baker, M. D.; Ozin, G. A.; Godber, J. *J. Phys. Chem.* **1985**, *89*, 305. Ozin, G. A.; Baker, D. M.; Godber, J. *J. Phys. Chem.* **1984**, *88*, 4902. Schoonheydt, R. A.; Hall, M. B.; Lunsford, J. H. *Inorg. Chem.* **1983**, *22*, 3834. Gellens, L. R.; Mortler, W. J.; Schoonheydt, R. A.; Uytterhoeven, J. B. *J. Phys. Chem.* **1981**, *85*, 2783. Kim, Y.; Seff, K. *J. Am. Chem. Soc.* **1978**, *100*, 6989.
- Kim, Y.; Seff, K. *J. Phys. Chem.* **1987**, *91*, 668.
- Calzaferri, G. *Photochemical and Photoelectrochemical Conversion and Storage of Solar Energy*; Tian, Z. W., Cao, Y., Eds.; International Academic Publishers: Beijing, 1993; p 141.
- Amblard, J.; Platzer, O.; Ridard, J.; Belloni, J. *J. Phys. Chem.* **1992**, *96*, 2341.
- Henglein, A. *Ber. Bunsen-Ges. Phys. Chem.* **1990**, *94*, 600.
- Plieth, W. J. *J. Phys. Chem.* **1982**, *86*, 3166.
- Brändle, M.; Calzaferri, G. *Res. Chem. Intermed.* **1994**, *20*, 783.
- Stein, A.; Ozin, G. A.; Stucky, D. D. *J. Am. Chem. Soc.* **1992**, *114*, 8119. Stein, A.; Ozin, G. A.; Macdonald, P. M.; Stucky, D. D. *J. Am. Chem. Soc.* **1992**, *114*, 5173.
- Calzaferri, G.; Gfeller, N.; Pfanner, K. *J. Photochem. Photobiol. A: Chem.* **1995**, *87*, 81.